

# Learning Only with Images: Visual Reinforcement Learning with Reasoning, Rendering, and Visual Feedback

Yang Chen<sup>1,2\*</sup>, Yufan Shen<sup>1\*†</sup>, Wenxuan Huang<sup>3</sup>, Shen Zhou<sup>2</sup>,  
Qunshu Lin<sup>4,2</sup>, Xinyu Cai<sup>1</sup>, Zhi Yu<sup>2†</sup>, Botian Shi<sup>1</sup>, Yu Qiao<sup>1</sup>

<sup>1</sup>Shanghai Artificial Intelligence Laboratory <sup>2</sup>Zhejiang University  
<sup>3</sup>East China Normal University <sup>4</sup>Abaka AI  
shenyfzju@gmail.com

## Abstract

Multimodal Large Language Models (MLLMs) have exhibited impressive performance across various visual tasks. Subsequent investigations into enhancing their visual reasoning abilities have significantly expanded their performance envelope. However, a critical bottleneck in the advancement of MLLMs toward deep visual reasoning is their heavy reliance on curated image-text supervision. To solve this problem, we introduce a novel framework termed “Reasoning-Rendering-Visual-Feedback” (RRVF), which enables MLLMs to learn complex visual reasoning from only raw images. This framework builds on the “Asymmetry of Verification” principle to train MLLMs, *i.e.*, verifying the rendered output against a source image is easier than generating it. We demonstrate that this relative ease provides an ideal reward signal for optimization via Reinforcement Learning (RL) training, reducing the reliance on the image-text supervision. Guided by the above principle, RRVF implements a closed-loop iterative process encompassing reasoning, rendering, and visual feedback components, enabling the model to perform self-correction through multi-turn interactions and tool invocation, while this pipeline can be optimized by the GRPO algorithm in an end-to-end manner. Extensive experiments on image-to-code generation for data charts and web interfaces show that RRVF substantially outperforms existing open-source MLLMs and surpasses supervised fine-tuning baselines. Our findings demonstrate that systems driven by purely visual feedback present a viable path toward more robust and generalizable reasoning models without requiring explicit supervision. Code will be available at <https://github.com/L-O-I/RRVF>.

## Introduction

Improving complex reasoning in Large Language Models (LLMs) represents a fundamental challenge in AI research and a critical milestone on the path to Artificial General Intelligence (AGI) (OpenAI 2024b; DeepSeek-AI et al. 2025; Hu et al. 2025; Team et al. 2025b). Recent works have attempted to replicate this success in Multimodal Large Language Models (MLLMs) for addressing complex visual tasks, yet this paradigm introduces several challenges (Huang et al. 2025; Shen et al. 2025a).

\*These authors contributed equally. Work done during Yang Chen’s internship at Shanghai Artificial Intelligence Laboratory.

†Corresponding Author

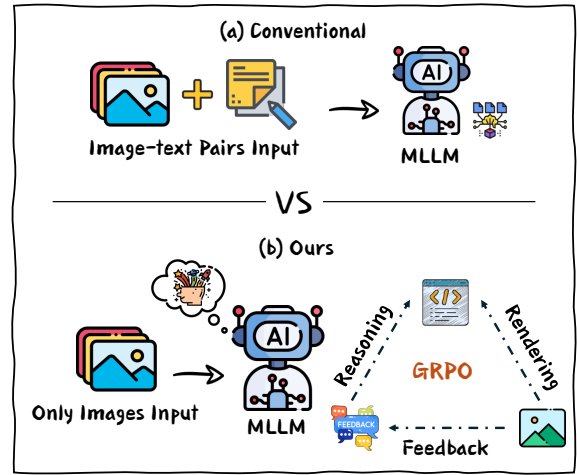


Figure 1: Comparison of training paradigms. Conventional MLLMs (top) rely on paired image-text data and learn by generating and verifying verbose, error-prone textual plans, whereas our RRVF framework (bottom) trains solely on raw images via a closed-loop reasoning-rendering-visual-feedback process under GRPO, inferring the underlying visual generation logic without text supervision.

Specifically, for MLLMs, effective reasoning necessitates capabilities that extend beyond elementary visual perception to achieve sophisticated visual comprehension and inference. This paradigm requires models to not only perform object recognition but also to analyze underlying visual semantics, spatial-geometric relationships, and complex inter-object dependencies (Su et al. 2025c; Luo et al. 2024). While accurate visual perception serves as a fundamental prerequisite for such reasoning capabilities, it inherently depends on robust reasoning mechanisms, creating a bidirectional dependency.

Recently, the pioneering work, like OpenAI’s “Think with Images” (OpenAI 2025b; Su et al. 2025a), has shown how external tools like OCR and zoom can enable models to interact proactively with visual content. Subsequent approaches expand beyond limited tool sets by generating executable code for visual operations through Reinforcement

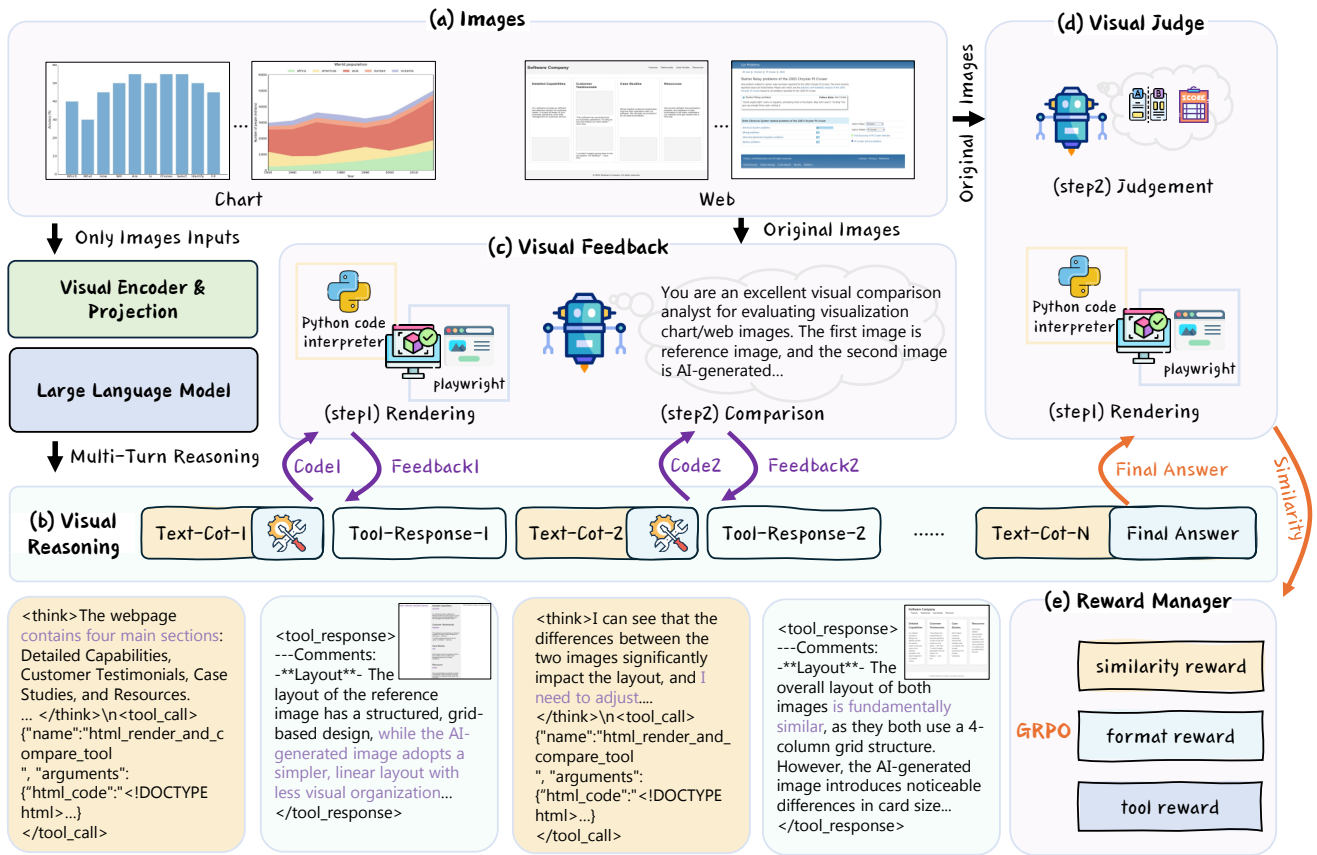


Figure 2: RRVF is a training framework that improves visual reasoning ability using only image inputs. Given an input image (a), the multimodal language model performs iterative reasoning (b) by generating rendering code. The code is executed by external tools, and the output is compared with the original image by a visual judge (d). The comparison results are converted into structured feedback (c), which guides the next round of code generation. The reward manager (e) combines visual similarity, format validity, and tool usage efficiency. These signals are used to optimize the model through reinforcement learning, implemented with the GRPO algorithm.

Learning (RL) training (Sutton, Barto et al. 1998), as seen in VRAG-RL (Wang et al. 2025b; Liu et al. 2025b). This demonstrates that incorporating external tools and reusing visual representations in MLLM reasoning can effectively enhance model performance.

Inspired by this, we propose an MLLM RL framework called “Reasoning-Rendering-Visual-Feedback” (RRVF) to endow MLLMs with enhanced visual comprehension and reasoning capabilities. As shown in Figure 1, this framework enhances visual understanding through a cycle of reasoning, rendering, and visual feedback, relying solely on images as training data. The core design is motivated by the “Asymmetry of Verification” principle (Wei 2025), *i.e.*, for many tasks, a proposed solution is substantially easier to verify than to generate. Specifically, tasks exhibiting this property are particularly amenable to RL training, as the efficient verification process can be directly formulated as a reward signal. Remarkably, we observe that for *image-to-code* tasks, *e.g.*, converting the chart image to the executable code, verifying the visual similarity between rendered outputs and source images proves substantially more tractable than gen-

erating rendering code from scratch.

Within the RRVF framework, the MLLM reasons about an input image to generate rendering code, which is then executed by a tool. Based on the visual discrepancy between the rendered and original images, the MLLM iteratively refines its code across multiple turns. To optimize this closed-loop refinement process, the system is modeled as a reinforcement learning task driven by the GRPO algorithm (Shao et al. 2024b). The learning is guided by a reward signal that incorporates the final visual similarity score. This mechanism compels the model to understand the image’s generative logic from raw pixels, leading to semantically correct code. The training process requires no text-based ground truth. This naturally resolves the “semantic equivalence” issue, as any program that produces the correct visual output is rewarded.

Moreover, the GRPO optimization is guided by a hybrid reward function. (1) The primary component is a visual similarity reward that quantifies the fidelity between the rendered image and the original image by integrating signals from established vision-language models. (2) This is supplemented

by a format correctness reward to ensure the generation of syntactically correct and executable code. And (3) an adaptive tool-use efficiency reward is introduced to balance exploration and convergence. This hybrid reward function effectively enables the model to learn underlying generative logic directly from pixel-level visual representations.

To demonstrate the effectiveness of the proposed RRVF framework, we evaluate our method in two distinct domains, data charts and web interfaces, while *using only raw pixel-based images as input*. Extensive experiments show that the RRVF framework enables MLLMs to effectively learn the underlying generative logic for both domains, capturing structures that range from the strict syntax of programming toolkits to the flexible layouts of web pages.

Our main contributions are as follows:

- We propose a novel RL training framework, RRVF, which can enhance MLLM visual reasoning through a Reasoning-Rendering-Visual-Feedback loop. By leveraging the “Asymmetry of Verification” principle, RRVF learns complex generative logic directly from only raw images, obviating the need for paired image-text supervision data.
- A structured feedback mechanism is introduced to convert unstructured visual discrepancies into actionable, multi-turn guidance signals. This mechanism enables iterative code refinement without textual supervision, while addressing semantic equivalence issues by rewarding visually faithful outputs. The distinct phases of the learned refinement behavior are also analyzed, revealing how the model evolves from exploration to efficient convergence.
- Extensive evaluation of the RRVF framework across two structurally diverse domains (*i.e.*, data charts and web UIs) demonstrates that the proposed approach successfully learns underlying generative logic directly from pixel-level representations and significantly outperforms existing baseline methods, establishing a promising paradigm for developing more capable and interpretable multimodal visual systems.

## Related Works

### Multimodal Large Models

Multimodal large models (Liu et al. 2023; Bai et al. 2025; Zhu et al. 2025; Anthropic 2025; OpenAI 2025a; Google 2025) are being iterated at high speed, especially showing excellent capabilities in visual information understanding and cross-modal interaction tasks. The powerful closed-source commercial models GPT-o3 (OpenAI 2025a) and Gemini-2.5 (Google 2025) use a unified Transformer architecture to achieve end-to-end processing of multimodal inputs such as images, text, and even long video sequences. This type of model significantly improves the perception and understanding abilities of intelligent systems for complex real-world scenes through deep fusion and collaborative reasoning of multi-source heterogeneous information, laying a solid foundation for its application in a wide range of fields. At the same time, the open source community

is also actively engaged in the exploration and innovation of MLLMs (Team et al. 2025c; Guo et al. 2025; Team et al. 2025a), and a series of influential research results have emerged (Shen et al. 2025a; Ma et al. 2025). For example, InternVL3 (Zhu et al. 2025) has set new performance records in many authoritative multimodal evaluation benchmarks with its strong visual encoder design and refined cross-modal alignment mechanism; models such as Qwen2.5-VL (Bai et al. 2025) have demonstrated unique advantages in multi-language support capabilities and specific visual tasks such as optical character recognition (OCR) and document intelligent understanding. These open-source works have enriched the technical ecology of MLLMs and promoted the democratization of related technologies (Chu et al. 2025; Liu et al. 2025a). Although existing MLLMs have made significant progress in enhancing the richness of visual representation learning and expanding the ability to process long context sequences, they still have limitations in deep visual reasoning and do not fully utilize visual information (Su et al. 2025c; Wang et al. 2025c).

### Visual Reasoning

Visual reasoning, as a core capability in multimodal understanding, has garnered significant attention from the academic community in recent years (Su et al. 2025c). Efforts to bridge the semantic gap between continuous visual information and discrete language have evolved through several stages: from encoding images into static visual features for Large Language Models (LLMs), to leveraging text-based Chain-of-Thought (CoT) for reasoning (Zhang et al. 2023; Wang et al. 2025c), which explicitly breaks down complex visual problems into textual intermediate steps (Shao et al. 2024a), and more recently, to accomplishing tasks by invoking external tools (Zheng et al. 2025; Xu et al. 2025; Wu et al. 2024b; Fu et al. 2025). This paradigm, where models learn to call APIs, was pioneered in language-only contexts by works like Toolformer (Schick et al. 2023) and extended to multimodal scenarios where models orchestrate various visual foundation models as tools (Wu et al. 2023). Building upon this, some models will act as advanced planners (Qi et al. 2024; Su et al. 2025b), enriching visual understanding at a finer-grained level by dynamically and iteratively invoking tools like “zoom in” and “crop” as reasoning steps. To further enhance the model’s autonomous cognitive abilities, subsequent research has transcended the limitations of predefined toolsets by generating executable visual code. This approach increases reasoning flexibility by decomposing complex visual tasks into modular and programmatic sub-tasks (Wang et al. 2025a; Mallis et al. 2024; Hu et al. 2024; Shen et al. 2025b; Surís, Menon, and Vondrick 2023). This has been a long-standing goal in areas like web UI generation (Beltramelli 2018) and has recently seen renewed interest in domains like data chart translation (Zhao et al. 2025). The generated code serves not only as a solution but also as a transparent representation of the model’s reasoning process, significantly enhancing its interpretability. Currently, the field of visual reasoning is undergoing a paradigm shift from static recognition towards structured, interactive, and explainable reasoning. This trend offers key

---

**Algorithm 1: Iterative Visual Reasoning**

---

**Require:** MLLM  $\mathcal{M}$ , Single Image  $I$ , Max Turns  $T_{max}$   
**Ensure:** Final rendering code  $C_{final}$

```
1:  $H \leftarrow \text{InitialPrompt}(I)$ 
2: for  $t = 1$  to  $T_{max}$  do
3:    $R_{model} \leftarrow \mathcal{M}.\text{Generate}(H)$   $\triangleright$  Generate response
4:    $H \leftarrow H \oplus R_{model}$ 
5:   if  $R_{model}$  contains  $\langle \text{answer} \rangle$  then
6:      $C_{final} \leftarrow \text{Extract}(R_{model}, \langle \text{answer} \rangle)$ 
7:     break  $\triangleright$  Final turn: task is complete
8:   else
9:      $C_{tool} \leftarrow \text{Extract}(R_{model}, \langle \text{tool\_call} \rangle)$ 
10:     $F \leftarrow \text{CallTool}(C_{tool})$   $\triangleright$  Invoke the external tool
11:     $H \leftarrow H \oplus F$   $\triangleright$  Append visual feedback to
    history
12:   end if
13: end for
14: return  $C_{final}$ 
```

---

insights for future research in visual understanding and self-supervised learning based on executable scenarios.

## Method

This section presents the Reasoning-Rendering-Visual-Feedback (RRVF) framework, a paradigm designed to enhance MLLM visual reasoning without text labels, through an iterative process. The overall architecture is detailed first, followed by the reinforcement learning strategy used for optimization.

### RRVF Framework

The core of RRVF is a closed-loop system comprising three key components: an iterative visual reasoner, a visual feedback mechanism, and a final visual judge.

**Visual Reasoning.** The process for generating rendering code is an iterative procedure, formally outlined in Algorithm 1. It begins with a single image input. In each turn, as illustrated in Figure 2(b), the MLLM produces a response (Line 3) that includes both internal reasoning in  $\langle \text{think} \rangle$  tags and a specific action. For intermediate turns, this action is a code snippet enclosed in a  $\langle \text{tool\_call} \rangle$  tag. A call is then made to an external tool to execute this code (Line 10). The resulting feedback is appended to the conversation history to inform the next turn. This iterative cycle concludes when the model’s response contains the final solution within an  $\langle \text{answer} \rangle$  tag, which terminates the process (Lines 5-7). The process also stops if a predefined maximum number of turns is reached (Yao et al. 2023; Madaan et al. 2023).

**Visual Feedback.** The visual feedback mechanism (Bai et al. 2022), illustrated in Figure 2(c), is a critical tool that provides structured guidance for the MLLM. Its operation involves two main steps:

- **Step 1: Rendering.** The code generated by the MLLM is executed by a specific rendering engine based on the domain. For data charts, Python code is executed using

libraries such as Matplotlib. For web interfaces, the Playwright library is utilized to render the HTML/CSS in a browser and capture a screenshot. In cases where the code is invalid and rendering fails, the tool returns an explicit failure signal.

- **Step 2: Comparison and Feedback Generation.** The successfully rendered image is compared to the original input image. This comparison is performed by a separate, powerful MLLM acting as a qualitative assessor. It is prompted to articulate the specific visual discrepancies (e.g., incorrect colors, misaligned elements, missing text) in natural language. This descriptive feedback provides actionable information for the primary MLLM’s next reasoning step.

**Visual Judge.** The Visual Judge (Figure 2(d)) provides a quantitative score for the final output, which is essential for policy optimization. The process first renders the final code and then uses a powerful MLLM to evaluate the similarity between the generated and target images (Zheng et al. 2023). The MLLM-based score serves as one of the reward signals for reinforcement learning and forms the primary optimization objective.

### Reinforcement Learning Optimization

For image-to-code generation tasks, the iterative and goal-oriented characteristics of the proposed RRVF framework render it particularly amenable to reinforcement learning formulations (Ouyang et al. 2022; Chen et al. 2021). The optimization process can be effectively formulated as learning an optimal policy that generates accurate rendering code, thereby enhancing the model’s fundamental visual understanding capabilities. Additionally, Group Relative Policy Optimization (GRPO) (Shao et al. 2024b) has been demonstrated to effectively guide model learning toward optimal trajectories through objective verification. Therefore, we employ GRPO as the optimization algorithm for RRVF to learn the capability of modeling rendering code by *verifying the visual similarity between rendered outputs and source images*. In the following sections, we provide a detailed description of our optimization algorithm.

**Optimization with GRPO.** The MLLM’s policy, denoted as  $\pi_\theta$ , is optimized using GRPO, which serves as a computationally efficient alternative to Proximal Policy Optimization (PPO) (Schulman et al. 2017). Unlike PPO, GRPO eliminates the need for a separate value function for advantage estimation, thereby avoiding high computational overhead and streamlining the optimization process by generating a set of candidate outputs from the previous policy iteration.

Specifically, GRPO samples a group of outputs  $\{o_1, o_2, \dots, o_G\}$  for each input query  $q$  from the old policy  $\pi_{\theta_{old}}$ . The method then optimizes the policy by maximizing a surrogate objective that incorporates clipping for stability, along with a KL regularization term to prevent excessive deviation from a reference policy  $\pi_{ref}$ . The objective function is given as:

Table 1: Performance comparison on the ChartMimic benchmark. We report compilation success (“Exec rate”), similarity scores for specific attributes, and a quality score from “GPT-4o”, which are the metrics from the original ChartMimic benchmark (Yang et al. 2024). The best results among open-source models under 10B parameters are **bolded**. Results marked with \* are reported by the original benchmark.

| Model                             | Exec rate    | Text         | Layout       | Type         | Color        | GPT-4o score | Overall      |
|-----------------------------------|--------------|--------------|--------------|--------------|--------------|--------------|--------------|
| <i>Closed-Source MLLMs</i>        |              |              |              |              |              |              |              |
| (2024/02) Gemini-1.0-Pro-Vision   | 68.2*        | 52.6*        | 64.2*        | 51.3*        | 47.1*        | 53.3*        | 53.6*        |
| (2024/11) GPT-4o-2024-11-20       | 90.00        | 66.55        | 79.31        | 71.83        | 60.84        | 82.50        | 76.06        |
| (2025/04) OpenAI O3               | 90.17        | 74.17        | 80.58        | 71.37        | 63.74        | 86.45        | 79.46        |
| (2025/05) Claude-4-Sonnet         | 91.83        | 68.87        | 82.43        | 67.13        | 57.59        | 85.46        | 77.23        |
| (2025/06) Gemini-2.5-Pro          | 93.33        | 84.95        | 83.37        | 75.05        | 66.90        | 90.58        | 84.07        |
| <i>Open-Source MLLMs</i>          |              |              |              |              |              |              |              |
| (2024/03) DeepSeek-VL-7B          | 41.3*        | 15.3*        | 26.6*        | 19.7*        | 14.5*        | 20.4*        | 19.7*        |
| (2025/02) LLaVA-OneVision-7B      | 17.28        | 7.97         | 13.55        | 9.15         | 7.36         | 10.01        | 9.76         |
| (2025/02) Qwen2.5-VL-7B-Instruct  | 68.83        | 30.01        | 55.79        | 36.50        | 26.91        | 39.04        | 38.17        |
| (2025/02) Qwen2.5-VL-72B-Instruct | 83.83        | 34.44        | 61.71        | 45.49        | 35.12        | 50.41        | 47.30        |
| (2025/04) InternVL3-8B            | 71.67        | 45.03        | 57.89        | 45.87        | 38.88        | 54.91        | 50.91        |
| SFT (5 epochs) [with text labels] | 69.00        | 56.97        | 63.60        | <b>60.53</b> | <b>51.89</b> | 62.09        | 60.17        |
| Δ (vs Qwen2.5-VL-7B-Instruct)     | +0.17        | +26.96       | +7.81        | +24.03       | +24.98       | +23.05       | +22.00       |
| RRVF (Ours) [without text labels] | <b>97.83</b> | <b>62.47</b> | <b>80.97</b> | 53.56        | 46.41        | <b>67.87</b> | <b>64.36</b> |
| Δ (vs Qwen2.5-VL-7B-Instruct)     | +29.00       | +32.46       | +25.18       | +17.06       | +19.50       | +28.83       | +26.19       |

$$\begin{aligned}
 J_{\text{GRPO}}(\theta) = & \mathbb{E}_{q \sim P(Q), \{o_i\}_{i=1}^G \sim \pi_{\theta_{\text{old}}}(O|q)} \\
 & \left[ \frac{1}{G} \sum_{i=1}^G \min\left(\frac{\pi_{\theta}(o_i | q)}{\pi_{\theta_{\text{old}}}(o_i | q)} A_i, \right. \right. \\
 & \left. \left. \text{clip}\left(\frac{\pi_{\theta}(o_i | q)}{\pi_{\theta_{\text{old}}}(o_i | q)}, 1 - \varepsilon, 1 + \varepsilon\right) A_i\right) \right. \\
 & \left. - \beta D_{\text{KL}}(\pi_{\theta} \parallel \pi_{\text{ref}}) \right], \quad (1)
 \end{aligned}$$

The advantage  $A_i$  is derived as a normalized relative measure:  $A_i = \frac{r_i - \text{mean}(\{r_1, r_2, \dots, r_G\})}{\text{std}(\{r_1, r_2, \dots, r_G\})}$ , using the rewards from the sampled group to establish a baseline. Additionally, the KL divergence term  $D_{\text{KL}}(\pi_{\theta} \parallel \pi_{\text{ref}})$  promotes controlled policy updates, balancing exploration and stability throughout training.

**Hybrid Reward Design.** As depicted in Figure 2(e), a hybrid reward function is engineered to provide a comprehensive learning signal. Our reward design necessitates the provision of dense and accurate reward signals to ensure format compliance during the model’s inference process while encouraging tool utilization to enhance the model’s performance ceiling. To address these objectives, we design the following three reward components:

- **Visual Similarity Reward ( $R_{\text{vision}}$ ):** This is the primary reward component, sourced directly from the Visual Judge module. It quantifies the fidelity between the final rendered image and the original input, providing a dense and accurate signal of task success. This reward can be efficiently computed using an MLLM as a judge,

thereby avoiding heavy reliance on curated image-text supervision.

- **Format Correctness Reward ( $R_{\text{format}}$ ):** This component provides a crucial binary signal that encourages the generation of valid and executable code. A positive reward is granted if the MLLM’s final code is syntactically correct and can be executed by the rendering engine without errors. Otherwise, a penalty is applied. This reward discourages the model from generating nonsensical or incomplete programs.
- **Tool-Use Reward ( $R_{\text{tool}}$ ):** This reward is designed to encourage tool use. It provides a small reward for each successful tool call, incentivizing the model to use the feedback loop to refine its answer. To avoid rewarding excessively long conversations, the reward is capped, balancing the need for exploration with the goal of convergence.

Furthermore, during RRVF training, we employ a weighted combination to balance these reward functions. The total reward  $R$  for a completed trajectory is a weighted sum of three distinct components:

$$R = w_v R_{\text{vision}} + w_f R_{\text{format}} + w_t R_{\text{tool}}, \quad (2)$$

where  $w_v$ ,  $w_f$ , and  $w_t$  are hyperparameters that balance the contribution of each component.

## Experiments

### Datasets and Evaluation

**Datasets and Metrics.** The framework’s performance is evaluated on two image-to-code tasks: chart-to-code and web-to-code. For the

Table 2: Performance comparison on the Plot2Code benchmark. We report metrics which are the original metrics from the plot2Code(Wu et al. 2024a). The “(fail=0)” scores are calculated by multiplying the original score by the execution rate, effectively giving a score of 0 to non-compiling code. The best results among open-source models under 10B parameters are **bolded**. Results marked with \* are reported by the original benchmark.

| Model                                | Exec rate    | Text         | GPT-4o Score | Text <sub>fail=0</sub> | GPT-4o Score <sub>fail=0</sub> |
|--------------------------------------|--------------|--------------|--------------|------------------------|--------------------------------|
| <i>Closed-Source MLLMs</i>           |              |              |              |                        |                                |
| (2023/09) GPT-4V                     | 84.1*        | 57.7*        | 6.48*        | 48.53*                 | 5.45*                          |
| (2024/02) Gemini-1.0-Pro-Vision      | 68.2*        | 53.6*        | 5.06*        | 36.56*                 | 3.45*                          |
| (2024/06) Claude-3-Sonnet            | 75.8*        | 46.7*        | 5.38*        | 35.40*                 | 4.08*                          |
| (2024/11) GPT-4o-2024-11-20          | 90.15        | 54.25        | 6.76         | 48.91                  | 6.09                           |
| (2025/04) OpenAI O3                  | 87.12        | 66.17        | 7.69         | 57.65                  | 6.70                           |
| (2025/05) Claude-4-Sonnet            | 92.42        | 61.52        | 6.76         | 56.86                  | 6.16                           |
| (2025/06) Gemini-2.5-Pro             | 87.88        | 81.59        | 8.71         | 71.70                  | 7.65                           |
| <i>Open-Source MLLMs</i>             |              |              |              |                        |                                |
| (2024/03) Mini-Gemini-8x7B-HD        | 73.5*        | 40.7*        | 3.87*        | 29.91*                 | 2.84*                          |
| (2025/02) LLaVA-OneVision-7B         | 84.09        | 31.78        | 3.27         | 26.72                  | 2.75                           |
| (2025/02) Qwen2.5-VL-7B-Instruct     | 70.46        | <b>50.81</b> | <b>4.82</b>  | 35.80                  | 3.40                           |
| (2025/02) Qwen2.5-VL-72B-Instruct    | 83.33        | 68.09        | 6.95         | 56.74                  | 5.79                           |
| (2025/04) InternVL3-8B               | 76.52        | 40.08        | 4.25         | 30.67                  | 3.25                           |
| <b>RRVF (Ours)</b>                   | <b>96.21</b> | 41.46        | 4.61         | <b>39.89</b>           | <b>4.44</b>                    |
| $\Delta$ (vs Qwen2.5-VL-7B-Instruct) | +25.75       | -9.35        | -0.21        | +4.09                  | +1.04                          |

Table 3: Performance comparison on the WebSight benchmark for web interface generation. “CLIP Score” measures the visual similarity between the generated output and the ground truth. The best results among open-source models under 10B parameters are **bolded**.

| Model                      | CLIP Score   | GPT Score    |
|----------------------------|--------------|--------------|
| <i>Closed-Source MLLMs</i> |              |              |
| GPT-4o                     | 88.94        | 94.55        |
| OpenAI O3                  | 91.58        | 96.49        |
| Claude-4-Sonnet            | 92.30        | 96.46        |
| Gemini-2.5-Pro             | 77.83        | 75.88        |
| <i>Open-Source MLLMs</i>   |              |              |
| LLaVA-OneVision-7B         | 79.74        | 72.61        |
| Qwen2.5-VL-7B              | 83.50        | 84.17        |
| InternVL3-8B               | 84.17        | 85.54        |
| <b>RRVF (Ours)</b>         | <b>85.95</b> | <b>86.52</b> |

chart-to-code task, two standard benchmarks are utilized. The official “chart-to-code” subset of the ChartMimic dataset (Yang et al. 2024) comprises 2,400 test images. From this set, 1,800 images are repurposed for training, while the remaining 600 images, which form the official smaller test set, are used for evaluation. Additionally, the Plot2Code dataset (Wu et al. 2024a), comprising 368 test cases, is used for zero-shot evaluation. For the web-to-code task, only 1,000 screenshots are randomly sampled from the WebSight dataset (Laurençon, Tronchon, and Sanh 2024) for training, with a disjoint set of 500

images reserved for testing.

For the chart-to-code task, evaluation adheres to the official protocols and metrics of its respective benchmarks. For the web-to-code task, however, traditional metrics such as block-level HTML comparisons are ill-suited for our framework. This is because the model is designed to generate semantically equivalent but structurally distinct code, without access to the ground-truth source. Consequently, evaluation for this task is based on visual fidelity and semantic correctness, quantified using the following metrics. (1) CLIP Similarity: The perceptual similarity between the rendered image and the original input is measured by the cosine similarity of their respective CLIP embeddings (Radford et al. 2021). (2) LLM-based Assessment: A powerful multi-modal model, GPT-4o (OpenAI 2024a), is employed as an impartial judge to assess the quality of the generated outputs. It evaluates semantic consistency, element completeness, and overall visual fidelity against the input image.

A comparison with conventional supervised fine-tuning approaches is presented in the ablation study.

**Baselines.** A comprehensive set of both closed-source and open-source models is selected for comparison to ensure a thorough evaluation. The closed-source baselines include leading proprietary models: GPT-4o (OpenAI 2024a), OpenAI O3 (OpenAI 2025a), Gemini-1.0-Pro-Vision (Google 2024), Gemini-2.5-Pro (Google 2025), and Claude-4-Sonnet (Anthropic 2025). The open-source counterparts include vision-language models such as Qwen2.5-VL (Bai et al. 2025), LLaVA-OneVision(Li et al. 2024a), Mini-Gemini (Li et al. 2024b), DeepSeek-VL (Lu et al. 2024), and InternVL3 (Zhu et al. 2025).

## Experimental Settings

**Training Setups.** The policy model is initialized from Qwen2.5-VL-Instruct-7B (Bai et al. 2025) and trained on a cluster of 8 NVIDIA A100 GPUs. The model is optimized using the GRPO algorithm with a global batch size of 32 and a learning rate of  $1 \times 10^{-6}$ . During each optimization step, a group of  $G = 8$  candidate trajectories is sampled for each prompt. The RRVF interaction loop is set to a maximum of 4 turns, and the maximum sequence length for generation is 16,384 tokens. The KL divergence coefficient is set to 0.0.

Visual feedback and judgment are provided by a more capable model, Qwen2.5-VL-Instruct-72B (Bai et al. 2025), which serves as the reward oracle. To handle the substantial computational demand during the policy rollout phase, this judge model is deployed on a separate, dedicated cluster of 8 NVIDIA A100 GPUs. Inference is accelerated using the vLLM framework (Kwon et al. 2023) to ensure high throughput for the large volume of verification requests generated in this process.

The optimization is guided by the hybrid reward function from Equation 2. The weights are set to  $w_v = -0.2$ ,  $w_f = 0.8$ , and  $w_t = 1.0$ . The interaction loop operates for a maximum of  $T_{max} = 4$  turns. Within this loop, the tool-use efficiency reward,  $R_{eff}$ , assigns a reward of 1/3 for each successful tool call and is fixed to its maximum value of 1.0 if the visual similarity score surpasses 0.95.

**Inference Setups.** During the evaluation phase, the model operates in a direct, single-turn inference mode. The final output is generated from the input prompt in a single pass, without access to the iterative refinement mechanism or any external tools available during the training loop. This protocol is intentionally designed to rigorously assess the model’s internalized multi-modal comprehension and generation capabilities, demonstrating the improvements gained autonomously after the completion of training.

## Main Results

The main experimental results are presented in Table 1, Table 2, and Table 3. The findings indicate that the RRVF-trained model achieves state-of-the-art performance among open-source Multimodal Large Language Models (MLLMs) of comparable size. This consistent outperformance across diverse tasks highlights the efficacy and generalizability of the proposed framework, which learns complex visual-to-code logic solely from visual feedback.

**Chart-to-Code Task.** On the ChartMimic benchmark (Table 1), the RRVF-trained model exhibits substantial improvements over its base model, Qwen2.5-VL-7B-Instruct. The most notable result is the code execution rate (*Exec rate*) of 97.83%, which surpasses all other evaluated models, including proprietary systems like OpenAI O3 and Gemini-2.5-Pro. This exceptional reliability in generating valid code is a direct result of the reinforcement learning process, which penalizes non-executable outputs. Consequently, the model attains an *Overall* score of 64.36, securing the highest performance among all open-source models. This performance is further supported by a strong score

in layout understanding (*Layout*: 80.97), suggesting that the visual feedback loop effectively teaches the model to infer and replicate the underlying structural logic of data visualizations.

On the Plot2Code dataset (Table 2), the RRVF model again achieves the highest execution rate (96.21%) among all competitors. It is crucial to interpret these results in the context of the benchmark’s evaluation protocol, where performance metrics are calculated only on successfully executed code. Due to its high execution rate, the RRVF model is evaluated on nearly the entire test set, including difficult instances where other models frequently fail to produce executable code. Models with lower execution rates are effectively scored on an easier subset of the data. Despite this more challenging evaluation condition, the RRVF model’s performance remains highly competitive. Moreover, if execution failures are penalized with 0 scores, RRVF still surpasses all similar-sized models, underscoring its enhanced robustness and reliability in generating correct code for a wider range of inputs.

**Web-to-Code Task.** The applicability of RRVF is further tested on the WebSight benchmark, a domain characterized by high structural freedom (Table 3). In this task, our RRVF-trained model achieves strong performance with a CLIP score of 85.95 and a GPT score of 86.52, surpassing the similar-sized models. Crucially, this advantage is obtained without any access to ground-truth HTML, relying instead on our proposed method. This demonstrates that the framework can effectively learn to deconstruct and replicate complex layouts and component relationships from raw pixels alone, validating the potential of learning through pure visual feedback even in highly unstructured domains.

## Ablation Study

An ablation study on the ChartMimic dataset directly compares RRVF against a standard Supervised fine-tuning (SFT) baseline, with both methods using the same Qwen2.5-VL-7B-Instruct base model. The results, presented in Table 1, show that RRVF substantially outperforms SFT, even though SFT has access to ground-truth code. The most significant gap lies in the code execution rate, where RRVF achieves **97.83%** versus SFT’s 69.00%. Furthermore, RRVF demonstrates a superior understanding of holistic visual structure, evidenced by its dominant *Layout* score (**80.97** vs. 63.60). This indicates that learning from the final visual outcome, as RRVF does, fosters a more robust and compositional understanding than simply imitating ground-truth code. This finding confirms that RRVF not only obviates the need for supervised labels but also surpasses the performance ceiling of standard imitation learning.

A particularly noteworthy finding emerges when comparing the final RRVF-trained model with the much larger Qwen2.5-VL-72B model, which serves as the visual judge providing feedback during training (see Table 1). The 7B model trained with RRVF achieves a higher *Overall* score than its 72B teacher (64.36 vs. 47.30). This counter-intuitive result is highly significant, as it demonstrates that the RRVF framework is not merely distilling the capabilities of the

judge model. Instead, the policy model uses the judge’s feedback as a reward signal to effectively explore the solution space and discover a superior policy. This proves that the performance of a model trained with RRVF is not fundamentally capped by the abilities of its feedback provider, highlighting the framework’s potential to bootstrap model capabilities beyond initial constraints.

## Limitations

The framework’s applicability is currently limited to code reconstruction tasks. Investigating the adaptation of RRVF to broader tasks, particularly those involving abstract reasoning where verification is non-trivial, remains an important avenue for future work.

## Conclusions

This paper presents RRVF, a framework that enhances visual reasoning in multimodal large language models through a reasoning-rendering-visual-feedback loop. The framework leverages the “Asymmetry of Verification” principle to learn generative logic directly from raw images, eliminating the need for paired textual supervision. Comprehensive experiments across charts and web interfaces show that RRVF consistently outperforms strong open-source baselines. The ablation study further confirms the superiority of the proposed framework over traditional supervised fine-tuning, validating its effectiveness in fostering robust visual reasoning.

## References

- Anthropic. 2025. Claude 4. <https://www.anthropic.com/news/claude-4/>. Accessed: 2025-07-24.
- Bai, S.; Chen, K.; Liu, X.; Wang, J.; Ge, W.; Song, S.; Dang, K.; Wang, P.; Wang, S.; Tang, J.; Zhong, H.; Zhu, Y.; Yang, M.; Li, Z.; Wan, J.; Wang, P.; Ding, W.; Fu, Z.; Xu, Y.; Ye, J.; Zhang, X.; Xie, T.; Cheng, Z.; Zhang, H.; Yang, Z.; Xu, H.; and Lin, J. 2025. Qwen2.5-VL Technical Report. arXiv:2502.13923.
- Bai, Y.; Kadavath, S.; Kundu, S.; Askell, A.; Kernion, J.; Jones, A.; Chen, A.; Goldie, A.; Mirhoseini, A.; McKinnon, C.; et al. 2022. Constitutional ai: Harmlessness from ai feedback. *arXiv preprint arXiv:2212.08073*.
- Beltramelli, T. 2018. pix2code: Generating code from a graphical user interface screenshot. In *Proceedings of the ACM SIGCHI symposium on engineering interactive computing systems*, 1–6.
- Chen, L.; Lu, K.; Rajeswaran, A.; Lee, K.; Grover, A.; Laskin, M.; Abbeel, P.; Srinivas, A.; and Mordatch, I. 2021. Decision transformer: Reinforcement learning via sequence modeling. *Advances in neural information processing systems*, 34: 15084–15097.
- Chu, T.; Zhai, Y.; Yang, J.; Tong, S.; Xie, S.; Schuurmans, D.; Le, Q. V.; Levine, S.; and Ma, Y. 2025. SFT Memorizes, RL Generalizes: A Comparative Study of Foundation Model Post-training. arXiv:2501.17161.
- DeepSeek-AI; Guo, D.; Yang, D.; Zhang, H.; Song, J.; Zhang, R.; and et al. 2025. DeepSeek-R1: Incentivizing Reasoning Capability in LLMs via Reinforcement Learning. arXiv:2501.12948.
- Fu, X.; Liu, M.; Yang, Z.; Corring, J.; Lu, Y.; Yang, J.; Roth, D.; Florencio, D.; and Zhang, C. 2025. Refocus: Visual editing as a chain of thought for structured image understanding. *arXiv preprint arXiv:2501.05452*.
- Google. 2024. GeminiProVision. <https://cloud.google.com/vertex-ai/generative-ai/docs/learn/model-versioning/>. Accessed: 2025-07-24.
- Google. 2025. Gemini-2-5-model-family. <https://blog.google/products/gemini/gemini-2-5-model-family-expands/>. Accessed: 2025-07-15.
- Guo, D.; Wu, F.; Zhu, F.; Leng, F.; Shi, G.; Chen, H.; Fan, H.; Wang, J.; Jiang, J.; and et al. 2025. Seed1.5-VL Technical Report. arXiv:2505.07062.
- Hu, J.; Zhang, Y.; Han, Q.; Jiang, D.; Zhang, X.; and Shum, H.-Y. 2025. Open-Reasoner-Zero: An Open Source Approach to Scaling Up Reinforcement Learning on the Base Model. arXiv:2503.24290.
- Hu, Y.; Stretcu, O.; Lu, C.-T.; Viswanathan, K.; Hata, K.; Luo, E.; Krishna, R.; and Fuxman, A. 2024. Visual program distillation: Distilling tools and programmatic reasoning into vision-language models. In *Proceedings of the IEEE/CVF Conference on Computer Vision and Pattern Recognition*, 9590–9601.
- Huang, W.; Jia, B.; Zhai, Z.; Cao, S.; Ye, Z.; Zhao, F.; Xu, Z.; Hu, Y.; and Lin, S. 2025. Vision-R1: Incentivizing Reasoning Capability in Multimodal Large Language Models. arXiv:2503.06749.
- Kwon, W.; Li, Z.; Zhuang, S.; Sheng, Y.; Zheng, L.; Yu, C. H.; Gonzalez, J. E.; Zhang, H.; and Stoica, I. 2023. Efficient Memory Management for Large Language Model Serving with PagedAttention. In *Proceedings of the ACM SIGOPS 29th Symposium on Operating Systems Principles*.
- Laurençon, H.; Tronchon, L.; and Sanh, V. 2024. Unlocking the conversion of web screenshots into html code with the websight dataset. *arXiv preprint arXiv:2403.09029*.
- Li, B.; Zhang, Y.; Guo, D.; Zhang, R.; Li, F.; Zhang, H.; Zhang, K.; Zhang, P.; Li, Y.; Liu, Z.; et al. 2024a. Llava-onevision: Easy visual task transfer. *arXiv preprint arXiv:2408.03326*.
- Li, Y.; Zhang, Y.; Wang, C.; Zhong, Z.; Chen, Y.; Chu, R.; Liu, S.; and Jia, J. 2024b. Mini-Gemini: Mining the Potential of Multi-modality Vision Language Models. arXiv:2403.18814.
- Liu, H.; Li, C.; Wu, Q.; and Lee, Y. J. 2023. Visual instruction tuning. *Advances in neural information processing systems*, 36: 34892–34916.
- Liu, Z.; Sun, Z.; Zang, Y.; Dong, X.; Cao, Y.; Duan, H.; Lin, D.; and Wang, J. 2025a. Visual-RFT: Visual Reinforcement Fine-Tuning. arXiv:2503.01785.
- Liu, Z.; Zang, Y.; Zou, Y.; Liang, Z.; Dong, X.; Cao, Y.; Duan, H.; Lin, D.; and Wang, J. 2025b. Visual Agentic Reinforcement Fine-Tuning. arXiv:2505.14246.
- Lu, H.; Liu, W.; Zhang, B.; Wang, B.; Dong, K.; Liu, B.; Sun, J.; Ren, T.; Li, Z.; Yang, H.; Sun, Y.; Deng, C.; Xu, H.;

- Xie, Z.; and Ruan, C. 2024. DeepSeek-VL: Towards Real-World Vision-Language Understanding. arXiv:2403.05525.
- Luo, C.; Shen, Y.; Zhu, Z.; Zheng, Q.; Yu, Z.; and Yao, C. 2024. Layoutlm: Layout instruction tuning with large language models for document understanding. In *Proceedings of the IEEE/CVF conference on computer vision and pattern recognition*, 15630–15640.
- Ma, Y.; Du, L.; Shen, X.; Chen, S.; Li, P.; Ren, Q.; Ma, L.; Dai, Y.; Liu, P.; and Yan, J. 2025. One RL to See Them All: Visual Triple Unified Reinforcement Learning. arXiv:2505.18129.
- Madaan, A.; Tandon, N.; Gupta, P.; Hallinan, S.; Gao, L.; Wiegrefe, S.; Alon, U.; Dziri, N.; Prabhunoye, S.; Yang, Y.; et al. 2023. Self-refine: Iterative refinement with self-feedback. *Advances in Neural Information Processing Systems*, 36: 46534–46594.
- Mallis, D.; Karadeniz, A. S.; Cavada, S.; Rukhovich, D.; Foteinopoulou, N.; Cherenkova, K.; Kacem, A.; and Aouada, D. 2024. Cad-assistant: Tool-augmented vlms as generic cad task solvers. *arXiv preprint arXiv:2412.13810*.
- OpenAI. 2024a. gpt-4o-and-more-tools-to-chatgpt-free. <https://openai.com/zh-Hans-CN/index/gpt-4o-and-more-tools-to-chatgpt-free/>. Accessed: 2025-07-24.
- OpenAI. 2024b. introducing-openai-o1-preview. <https://openai.com/zh-Hans-CN/index/introducing-openai-o1-preview/>. Accessed: 2025-07-24.
- OpenAI. 2025a. Introducing-o3-and-o4-mini. <https://openai.com/zh-Hans-CN/index/introducing-o3-and-o4-mini/>. Accessed: 2025-07-15.
- OpenAI. 2025b. Thinking with images. <https://openai.com/index/thinking-with-images/>. Accessed: 2025-07-15.
- Ouyang, L.; Wu, J.; Jiang, X.; Almeida, D.; Wainwright, C.; Mishkin, P.; Zhang, C.; Agarwal, S.; Slama, K.; Ray, A.; et al. 2022. Training language models to follow instructions with human feedback. *Advances in neural information processing systems*, 35: 27730–27744.
- Qi, J.; Ding, M.; Wang, W.; Bai, Y.; Lv, Q.; Hong, W.; Xu, B.; Hou, L.; Li, J.; Dong, Y.; et al. 2024. Cogcom: Train large vision-language models diving into details through chain of manipulations.
- Radford, A.; Kim, J. W.; Hallacy, C.; Ramesh, A.; Goh, G.; Agarwal, S.; Sastry, G.; Askell, A.; Mishkin, P.; Clark, J.; et al. 2021. Learning transferable visual models from natural language supervision. In *International conference on machine learning*, 8748–8763. PmLR.
- Schick, T.; Dwivedi-Yu, J.; Dessi, R.; Raileanu, R.; Lomeli, M.; Zettlemoyer, L.; Cancedda, N.; and Scialom, T. 2023. Toolformer: Language models can teach themselves to use tools, 2023. *arXiv preprint arXiv:2302.04761*.
- Schulman, J.; Wolski, F.; Dhariwal, P.; Radford, A.; and Klimov, O. 2017. Proximal policy optimization algorithms. *arXiv preprint arXiv:1707.06347*.
- Shao, H.; Qian, S.; Xiao, H.; Song, G.; Zong, Z.; Wang, L.; Liu, Y.; and Li, H. 2024a. Visual cot: Advancing multimodal language models with a comprehensive dataset and benchmark for chain-of-thought reasoning. *Advances in Neural Information Processing Systems*, 37: 8612–8642.
- Shao, Z.; Wang, P.; Zhu, Q.; Xu, R.; Song, J.; Bi, X.; Zhang, H.; Zhang, M.; Li, Y. K.; Wu, Y.; and Guo, D. 2024b. DeepSeekMath: Pushing the Limits of Mathematical Reasoning in Open Language Models. arXiv:2402.03300.
- Shen, H.; Liu, P.; Li, J.; Fang, C.; Ma, Y.; Liao, J.; Shen, Q.; Zhang, Z.; Zhao, K.; Zhang, Q.; Xu, R.; and Zhao, T. 2025a. VLM-R1: A Stable and Generalizable R1-style Large Vision-Language Model. arXiv:2504.07615.
- Shen, Y.; Luo, C.; Zhu, Z.; Chen, Y.; Zheng, Q.; Yu, Z.; Bu, J.; and Yao, C. 2025b. Proctag: Process tagging for assessing the efficacy of document instruction data. In *Proceedings of the AAAI Conference on Artificial Intelligence*, volume 39, 6851–6859.
- Su, A.; Wang, H.; Ren, W.; Lin, F.; and Chen, W. 2025a. Pixel Reasoner: Incentivizing Pixel-Space Reasoning with Curiosity-Driven Reinforcement Learning. arXiv:2505.15966.
- Su, Z.; Li, L.; Song, M.; Hao, Y.; Yang, Z.; Zhang, J.; Chen, G.; Gu, J.; Li, J.; Qu, X.; et al. 2025b. Openthinking: Learning to think with images via visual tool reinforcement learning. *arXiv preprint arXiv:2505.08617*.
- Su, Z.; Xia, P.; Guo, H.; Liu, Z.; Ma, Y.; Qu, X.; Liu, J.; Li, Y.; Zeng, K.; Yang, Z.; Li, L.; Cheng, Y.; Ji, H.; He, J.; and Fung, Y. R. 2025c. Thinking with Images for Multimodal Reasoning: Foundations, Methods, and Future Frontiers. arXiv:2506.23918.
- Surís, D.; Menon, S.; and Vondrick, C. 2023. Vipergpt: Visual inference via python execution for reasoning. In *Proceedings of the IEEE/CVF international conference on computer vision*, 11888–11898.
- Sutton, R. S.; Barto, A. G.; et al. 1998. *Reinforcement learning: An introduction*, volume 1. MIT press Cambridge.
- Team, C.; Yue, Z.; Lin, Z.; Song, Y.; Wang, W.; Ren, S.; Gu, S.; Li, S.; Li, P.; Zhao, L.; Li, L.; Bao, K.; Tian, H.; Zhang, H.; Wang, G.; Zhu, D.; Cici, He, C.; Ye, B.; Shen, B.; Zhang, Z.; Jiang, Z.; Zheng, Z.; Song, Z.; Luo, Z.; Yu, Y.; Wang, Y.; Tian, Y.; Tu, Y.; Yan, Y.; Huang, Y.; Wang, X.; Xu, X.; Song, X.; Zhang, X.; Yong, X.; Zhang, X.; Deng, X.; Yang, W.; Ma, W.; Lv, W.; Zhuang, W.; Liu, W.; Deng, S.; Liu, S.; Chen, S.; Yu, S.; Liu, S.; Wang, S.; Ma, R.; Wang, Q.; Wang, P.; Chen, N.; Zhu, M.; Zhou, K.; Zhou, K.; Fang, K.; Shi, J.; Dong, J.; Xiao, J.; Xu, J.; Liu, H.; Xu, H.; Qu, H.; Zhao, H.; Lv, H.; Wang, G.; Zhang, D.; Zhang, D.; Zhang, D.; Ma, C.; Liu, C.; Cai, C.; and Xia, B. 2025a. MiMo-VL Technical Report. arXiv:2506.03569.
- Team, K.; Du, A.; Gao, B.; Xing, B.; Jiang, C.; Chen, C.; Li, C.; and et al. 2025b. Kimi k1.5: Scaling Reinforcement Learning with LLMs. arXiv:2501.12599.
- Team, V.; Hong, W.; Yu, W.; Gu, X.; Wang, G.; Gan, G.; Tang, H.; Cheng, J.; Qi, J.; and et al. 2025c. GLM-4.1V-Thinking: Towards Versatile Multimodal Reasoning with Scalable Reinforcement Learning. arXiv:2507.01006.
- Wang, K.; Pan, J.; Wei, L.; Zhou, A.; Shi, W.; Lu, Z.; Xiao, H.; Yang, Y.; Ren, H.; Zhan, M.; et al. 2025a. MathCoder-VL: Bridging Vision and Code for Enhanced Multimodal Mathematical Reasoning. *arXiv preprint arXiv:2505.10557*.

Wang, Q.; Ding, R.; Zeng, Y.; Chen, Z.; Chen, L.; Wang, S.; Xie, P.; Huang, F.; and Zhao, F. 2025b. VRAG-RL: Empower Vision-Perception-Based RAG for Visually Rich Information Understanding via Iterative Reasoning with Reinforcement Learning. *arXiv:2505.22019*.

Wang, Y.; Wu, S.; Zhang, Y.; Yan, S.; Liu, Z.; Luo, J.; and Fei, H. 2025c. Multimodal chain-of-thought reasoning: A comprehensive survey. *arXiv preprint arXiv:2503.12605*.

Wei, J. 2025. The Asymmetry of Verification, and Verifier's Law. <https://www.jasonwei.net/blog/asymmetry-of-verification-and-verifiers-law>. Accessed: 2025-07-15.

Wu, C.; Ge, Y.; Guo, Q.; Wang, J.; Liang, Z.; Lu, Z.; Shan, Y.; and Luo, P. 2024a. Plot2code: A comprehensive benchmark for evaluating multi-modal large language models in code generation from scientific plots. *arXiv preprint arXiv:2405.07990*.

Wu, C.; Yin, S.; Qi, W.; Wang, X.; Tang, Z.; and Duan, N. 2023. Visual chatgpt: Talking, drawing and editing with visual foundation models. *arXiv preprint arXiv:2303.04671*.

Wu, Y.; Wang, Y.; Tang, S.; Wu, W.; He, T.; Ouyang, W.; Torr, P.; and Wu, J. 2024b. Dettoolchain: A new prompting paradigm to unleash detection ability of mllm. In *European Conference on Computer Vision*, 164–182. Springer.

Xu, C.; Wang, Y.; Wei, L.; Sun, L.; and Huang, W. 2025. Improved Iterative Refinement for Chart-to-Code Generation via Structured Instruction. *arXiv:2506.14837*.

Yang, C.; Shi, C.; Liu, Y.; Shui, B.; Wang, J.; Jing, M.; Xu, L.; Zhu, X.; Li, S.; Zhang, Y.; et al. 2024. Chartmimic: Evaluating lmm's cross-modal reasoning capability via chart-to-code generation. *arXiv preprint arXiv:2406.09961*.

Yao, S.; Zhao, J.; Yu, D.; Du, N.; Shafran, I.; Narasimhan, K.; and Cao, Y. 2023. React: Synergizing reasoning and acting in language models. In *International Conference on Learning Representations (ICLR)*.

Zhang, Z.; Zhang, A.; Li, M.; Zhao, H.; Karypis, G.; and Smola, A. 2023. Multimodal chain-of-thought reasoning in language models. *arXiv preprint arXiv:2302.00923*.

Zhao, X.; Luo, X.; Shi, Q.; Chen, C.; Wang, S.; Liu, Z.; and Sun, M. 2025. Chartcoder: Advancing multimodal large language model for chart-to-code generation. *arXiv preprint arXiv:2501.06598*.

Zheng, L.; Chiang, W.-L.; Sheng, Y.; Zhuang, S.; Wu, Z.; Zhuang, Y.; Lin, Z.; Li, Z.; Li, D.; Xing, E.; et al. 2023. Judging llm-as-a-judge with mt-bench and chatbot arena. *Advances in neural information processing systems*, 36: 46595–46623.

Zheng, Z.; Yang, M.; Hong, J.; Zhao, C.; Xu, G.; Yang, L.; Shen, C.; and Yu, X. 2025. DeepEyes: Incentivizing "Thinking with Images" via Reinforcement Learning. *arXiv:2505.14362*.

Zhu, J.; Wang, W.; Chen, Z.; Liu, Z.; Ye, S.; Gu, L.; Tian, H.; Duan, Y.; Su, W.; Shao, J.; et al. 2025. InternV13: Exploring advanced training and test-time recipes for open-source multimodal models. *arXiv preprint arXiv:2504.10479*.